
Using Synthetic Images to Augment Small Medical Image Datasets

Minh H. Vu

Department of Diagnostics and Intervention
Umeå University
minh.vu@umu.se

Lorenzo Tronchin

Università Campus Bio-Medico di Roma
l.tronchin@unicampus.it

Tufve Nyholm

Department of Diagnostics and Intervention
Umeå University
tufve.nyholm@umu.se

Tommy Löfstedt

Department of Computing Science
Umeå University
tommy.lofstedt@umu.se

Abstract

Recent years have witnessed a growing academic and industrial interest in deep learning (DL) for medical imaging. To perform well, DL models require very large labeled datasets. However, most medical imaging datasets are small, with a limited number of annotated samples. The reason they are small is usually because delineating medical images is time-consuming and demanding for oncologists. There are various techniques that can be used to augment a dataset, for example, to apply affine transformations or elastic transformations to available images, or to add synthetic images generated by a Generative Adversarial Network (GAN). In this work, we have developed a novel conditional variant of a current GAN method, the StyleGAN2, to generate multi-modal high-resolution medical images with the purpose to augment small medical imaging datasets with these synthetic images. We use the synthetic and real images from six datasets to train models for the downstream task of semantic segmentation. The quality of the generated medical images and the effect of this augmentation on the segmentation performance were evaluated afterward. Finally, the results indicate that the downstream segmentation models did not benefit from the generated images. Further work and analyses are required to establish how this augmentation affects the segmentation performance.

1 Introduction

There has been a recent surge in the interest in deep learning (DL) for medical imaging. This is partly due to the advancements in computing power (and storage), the availability of large datasets, and recent methodological and technical developments in the area. Computer vision, speech recognition, natural language processing, and bioinformatics are a few areas where DL has been put to use, with results obtained that are on par with, and in some cases better than, those achieved by human experts [Kühl et al., 2022]. DL has been used widely in the medical imaging field since DL models can be used to perform diagnosis and other tasks by directly interpreting medical images.

Deep generative models are a particular type of DL models that can learn a distribution over arbitrary data, *e.g.* over medical images. A Generative Adversarial Network (GAN) is a development in deep generative modeling [Goodfellow et al., 2014] that has seen substantial interest in the last years. In this work, we explore the potential of using GANs to augment small medical image datasets with synthetic images for the task of medical image segmentation.

A GAN model contains two (neural network) models, a generator and a discriminator [Goodfellow et al., 2014]. The generator attempts to generate synthetic but realistic samples such that the discriminator will mistake these generated samples for real samples. The discriminator is, on the other hand, trained to determine whether a given sample is generated or actual real data. In other words, the generator is not tasked with minimizing some distance to a target image or so but is instead trained to fool the discriminator. This makes it possible for the model to learn without supervision. The generator and the discriminator are trained in an alternating min-max procedure where the generator tries to minimize the discriminator’s ability to distinguish generated images from real, and the discriminator attempts to maximize its own ability to discriminate generated samples from real. The distribution of the generated samples should ideally be identical to the training data distribution after training, and it can be shown that the min-max training procedure can achieve this [Goodfellow et al., 2014]. In most cases, the generator is the primary focus, and the discriminator is often discarded once the generator has been trained.

Intriguing GAN applications include generating images in the style of another image [image-to-image translation, Han et al., 2018], image inpainting [filling in missing parts of an image, Armanious et al., 2019], and data augmentation [generating synthetic training data, Calimeri et al., 2017, Madani et al., 2018, Bowles et al., 2018, Kim et al., 2021, Motamed et al., 2021, Sandfort et al., 2019].

One of the main problems in medical imaging is having small datasets, with a limited number of annotated samples. This problem is emphasized in applications with DL since DL models need large labeled datasets. Experts, with extensive expertise in the data and the task at hand, often create annotations for medical imaging projects. It is often time-consuming to make these medical image annotations, particularly so for detailed annotations, such as segmentations of organs or lesions in many 2D slices of a 3D volume. Even though medical datasets are publicly accessible online, the majority of datasets are still limited in size and are only relevant for the specific medical concerns it was collected for.

The use of data augmentation is one strategy that researchers are pursuing to address this dilemma [*i.e.*, the dilemma of having datasets with limited sizes, Shorten and Khoshgoftaar, 2019]. The most used data augmentation techniques involve applying various spatial transformations to the original dataset, such as translation, rotation, flip, and scale, or color transformations, such as randomly changing an image’s hue, saturation, brightness, and contrast. These methods take advantage of changes that we know should not change the image’s assigned class. This method is very effective for small datasets. Even models trained on some of the largest publicly available datasets, such as the ImageNet dataset [Deng et al., 2009], can benefit from this method [Shorten and Khoshgoftaar, 2019]. In computer vision tasks, it is customary to use conventional data augmentation to assist the training process of neural network models. However, small transformations of images may not add much extra information (*e.g.*, the translation of an image by a few pixels). A novel and advanced data augmentation technique is to do data augmentation with high-quality and high-resolution generated synthetic images [Karras et al., 2018a,b, 2020b]. Synthetic images, or other data, created using a generative model may provide data with greater diversity that enriches the training data and improve the final model.

The main contributions of this work can be summarized as follows:

1. We propose a novel conditional GAN based on the StyleGAN2 model and refer to it as a “Conditional-StyleGAN2 model”.
2. We have systematically investigated the StyleGAN2 [Karras et al., 2020b] and the proposed Conditional-StyleGAN2.

2 Related Work

It is challenging to generate images with a high resolution; because the higher the resolution of an image, the easier it is for the discriminator to distinguish between “fake” and “real” images. Smaller mini-batches, that decrease the stability of the model training, and memory limits on commodity Graphical Processing Units (GPUs) are also two problems of generating high-resolution images [Odena et al., 2017]. Karras et al. [2018a] addressed this issue by proposing the progressive growing of GAN (Progressive-GAN). Their key contribution was to progressively increase the resolution of both the generator output and the discriminator input, beginning with low-resolution

images and successively adding new and larger layers that produce higher-resolution images. This significantly improved the generated image quality, accelerated the training, and improved the stability of training when generating high-resolution images. Karras et al. [2018b] later proposed the StyleGAN as a combination of Progressive-GAN [Karras et al., 2018a] and what’s called neural style transfer [*i.e.*, to copy the style of a source image to a new target image, Gatys et al., 2016]. A standard generator takes a latent code (a random noise vector) as an input, but Karras et al. [2018b] also proposed to map this latent input to an intermediate latent space that has fewer problems of entanglement between variables in the input latent space—*i.e.*, dimensions in the intermediate space are more likely to encode only a single feature. The intermediate latent vectors are then fed into a generator at multiple positions.

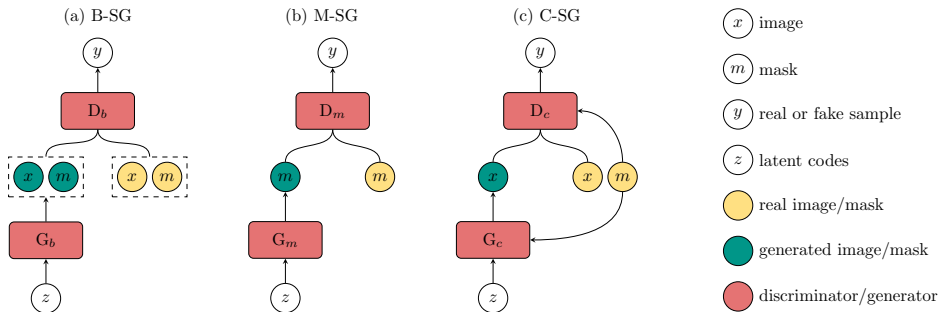


Figure 1: Comparison of GANs used in this work.

Karras et al. [2020b] further proposed the StyleGAN2, an improvement that restructures the normalization of the generator and also regularizes the generator. The restructuring improved the generated images’ quality, and their *path length regularizer* made the generator simpler to invert (to find the latent code that corresponds to an image). In follow-up work, Karras et al. [2020a] proposed the StyleGAN2-ADA to address the problem of overfitting the discriminator, which causes training to diverge due to insufficient data. In that work, they presented an adaptive discriminator augmentation approach that controls the stability of training on datasets with limited data. The StyleGAN2-ADA did not introduce any other modifications to the loss functions or the network designs. In a recent work, Karras et al. [2021] introduced the StyleGAN3, that eliminates *texture sticking*, induced by point-wise nonlinearities. Texture sticking happens when a generator memorizes a certain area’s textural features. To address the issue of texture sticking, Karras et al. [2021] also proposed interpreting all network signals as continuous and applying low-pass filters on these signals.

The conditional GAN was first introduced by Mirza and Osindero [2014] as a conditional version of the original GAN [Goodfellow et al., 2014]. The idea is to generate images given some piece of information, such as a desired label. Practically, this was achieved by passing the desired label as an input to the generator and the discriminator to inform about what was to be generated. Isola et al. [2017] extended the idea of a conditional GAN by conditioning on a source image to generate a target image and presented an image-to-image translation model called pix2pix (for pixel-to-pixel translation). They demonstrated that the pix2pix model is effective for various image translation applications, and one of these was image synthesis from binary label maps. Bailo et al. [2019] applied image-to-image translation on blood smear data to generate new samples and substantially expanded their small datasets. In particular, given the mask of a microscopy image, they generated high-quality blood cell samples, which were then used in conjunction with real data during network training for segmentation and object detection tasks.

GANs have been utilized for data augmentation to improve the training of Convolutional Neural Networks (CNNs) by generating additional samples from the training data distribution. Calimeri et al. [2017] proposed to use a GAN to generate magnetic resonance imaging (MRI) slices of the human brain. In another work, Madani et al. [2018] investigated using GANs to augment chest X-ray images that were then used when training a CNN for cardiovascular abnormality classification. Sandfort et al. [2019] used CycleGAN [Zhu et al., 2017] to generate contrast computed tomography (CT) from non-contrast CT images. In all these works above, they showed that using GAN to generate additional data for augmentation can provide significant improvements to the downstream task (*e.g.*, for segmentation or classification). Skandarani et al. [2021], however, argued that no GAN is capable of reproducing the full richness of medical datasets. In specific, despite being trained on

a significantly larger number of samples (real and generated), none of the segmentation networks’ performance match or surpass those trained on only the real data.

3 Proposed Methods

GANs are generative models that map a random noise vector, z , to an output sample (*e.g.*, an image). Depending on the problem, the output image can be a gray image [Goodfellow et al., 2014], a color image [Karras et al., 2020b], or a multi-modal medical images [Zhu et al., 2017]. The primary aim of this paper is to detail a proposition to use GANs to generate medical images and their corresponding label masks. We trained GANs on an existing dataset and used the generated synthetic samples, pairs that included both medical images (single-modal or multi-modal) and their masks, to enlarge the dataset for the downstream task of semantic segmentation. We trained a U-Net [Ronneberger et al., 2015] on the real samples and generated samples for the downstream task. We hypothesized that the segmentation performance when training on real and augmented samples (*i.e.*, generated images and masks) would be higher than when training on only real samples.

3.1 Objective

In this work, we propose two GANs based on the StyleGAN2 [Karras et al., 2020b]. The first StyleGAN2 was trained to generate label masks and is referred to as Mask StyleGAN2 (M-SG). The second GAN was a conditional variant of StyleGAN2 and is referred to as Conditional StyleGAN2 (C-SG). The condition for C-SG was the label mask. At the same time, the output of C-SG’s generator was that mask’s corresponding medical images. Third, we also use a standard, or baseline StyleGAN2, referred to as Baseline StyleGAN2 (B-SG), to generate a pair of medical images and label masks. We considered the B-SG as the baseline GAN model. Figure 1 illustrates the three GAN models considered in this work. We detail the three GANs below.

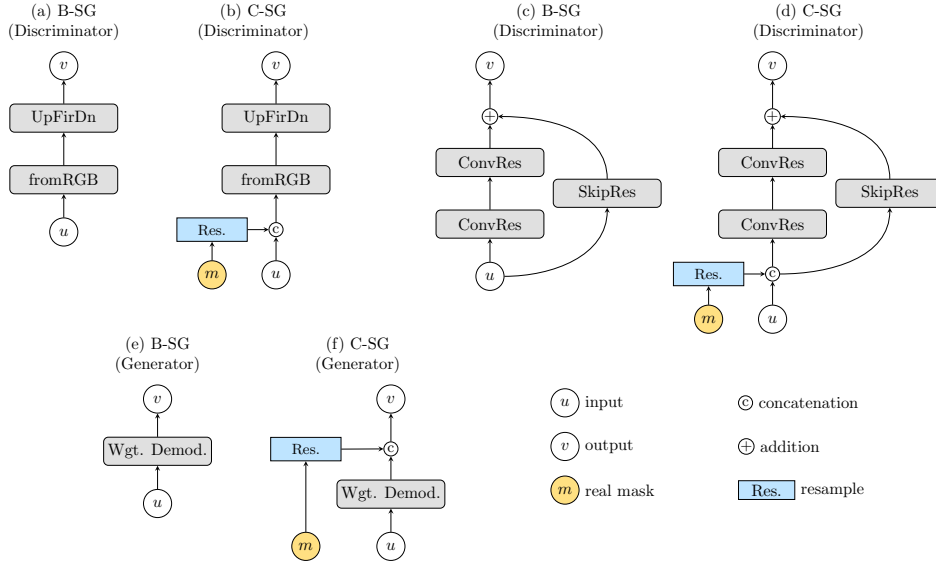


Figure 2: Comparison of architectures of B-SG (or M-SG) and C-SG. The “Wgt. Demod.” denote the weight demodulation module proposed by Karras et al. [2020b].

Let the training dataset be

$$\mathbf{F} = \{(\mathbf{x}_i, \mathbf{m}_i) : \forall i \in \{1, \dots, N\}\},$$

where N is the number of training pairs. The $(\mathbf{x}_i, \mathbf{m}_i)$ denotes the i -th training pair with an image, \mathbf{x}_i , and its corresponding label mask, \mathbf{m}_i .

We construct the label mask training set from \mathbf{F} as

$$\mathbf{M} = \{\mathbf{m}_i : (\mathbf{x}_i, \mathbf{m}_i) \in \mathbf{F}\}.$$

For the B-SG, the objective function of a two-player min-max game [Goodfellow et al., 2014] can be defined as

$$\min_{G_b} \max_{D_b} V(G_b, D_b) = \mathbb{E}_{(\mathbf{x}, \mathbf{m}) \sim p_{\mathbf{F}}(\mathbf{x}, \mathbf{m})} [\log D_b(\mathbf{x}, \mathbf{m})] + \mathbb{E}_{\mathbf{z} \sim p_{\mathbf{z}}(\mathbf{z})} [\log(1 - D_b(G_b(\mathbf{z})))]. \quad (1)$$

with G_b and D_b the generator and discriminator of the B-SG. The $p_{\mathbf{F}}(\mathbf{x}, \mathbf{m})$ denotes the underlying data distribution of the training data in \mathbf{F} , while $p_{\mathbf{z}}(\mathbf{z})$ is a prior on the latent noise vectors.

The objective function of the proposed M-SG is also a two-player min-max game and can be written as

$$\min_{G_m} \max_{D_m} V(G_m, D_m) = \mathbb{E}_{\mathbf{m} \sim p_{\mathbf{M}}(\mathbf{m})} [\log D_m(\mathbf{m})] + \mathbb{E}_{\mathbf{z} \sim p_{\mathbf{z}}(\mathbf{z})} [\log(1 - D_m(G_m(\mathbf{z})))], \quad (2)$$

with G_m and D_m the generator and discriminator of the M-SG. The $p_{\mathbf{M}}(\mathbf{m})$ denotes the underlying data distribution of training masks in \mathbf{M} , and $p_{\mathbf{z}}(\mathbf{z})$ is again a prior on the latent noise vectors.

Furthermore, we define the objective function of the proposed C-SG as

$$\min_{G_c} \max_{D_c} V(G_c, D_c) = \mathbb{E}_{(\mathbf{x}, \mathbf{m}) \sim p_{\mathbf{F}}(\mathbf{x}, \mathbf{m})} [\log D_c(\mathbf{x}|\mathbf{m})] + \mathbb{E}_{\mathbf{z} \sim p_{\mathbf{z}}(\mathbf{z})} [\log(1 - D_c(G_c(\mathbf{z}|\mathbf{m})))], \quad (3)$$

with G_c and D_c the generator and discriminator of the C-SG.

3.2 Conditional StyleGAN2 (C-SG)

Basically, B-SG and M-SG use the same architecture as the StyleGAN2. The only difference between B-SG and M-SG is the output of the generator, *i.e.* the output of B-SG is pairs of both the label masks and the medical images. In contrast, the output of M-SG is only the label masks.

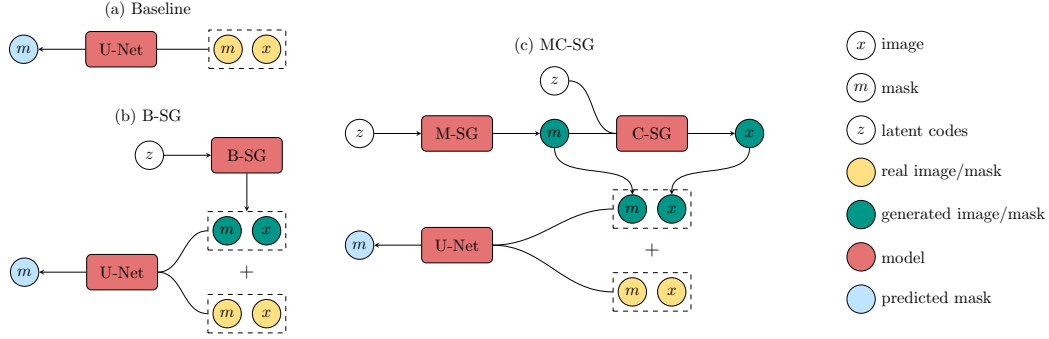


Figure 3: Proposed pipeline.

In order to use a condition as a mask in StyleGAN2, we introduce the C-SG. Figure 2 shows a comparison between the design of the B-SG (also M-SG) and of the proposed C-SG. From Figure 2, we can see that the C-SG differs the B-SG on three primary blocks: two in the discriminator (Figure 2(a)–Figure 2(d)) and one in the generator (Figure 2(e)–Figure 2(f)).

To incorporate the condition of the mask on the generated output in the generator, we feed a mask into the generator (see Figure 2(f)). In the C-SG, we resampled the label mask to the shape of the output of the weight demodulation module proposed by Karras et al. [2020b]. The resampled mask is then concatenated with the output of the weight demodulation module.

In the discriminator of C-SG, we provided the mask condition at two locations (see Figure 2(b) and Figure 2(d)). First, we concatenated the resampled mask with the input before it was fed into a layer called “fromRGB”. The “fromRGB” is a layer that converts an RGB image to a feature map. This layer, together with “toRGB”, that converts a feature map to an RGB image, was first introduced for the Progressive-GAN [Karras et al., 2018a]. The output of the concatenation operation was then fed

into a block named “UpFirDn”. The “UpFirDn” block includes a padding operation, an upsampling operation, a filtering operation with a given finite impulse response (FIR) filter, and followed by a downsampling operation. Second, we concatenated the resampled mask with the input before it was fed into a ResNet-like block [see Figure 2(d), He et al., 2016]. The ResNet-like block consisted of six components: two convolutional layers followed by two resampling layers and a skip connection followed by a resampling layer.

3.3 Proposed Pipeline

In this work, the downstream task is the semantic segmentation of medical images. The segmentation network used in this work was the U-Net [Ronneberger et al., 2015]. We split each dataset into three parts: training (60%), validation (20%), and test (20%). Figure 3 shows a comparison of three segmentation pipelines as follows. First, the baseline (BL) that utilized the U-Net to train only on the real samples (see Figure 3(a)). Second, the B-SG generated pairs of images and label masks. After that, the generated and the real samples were used to train the U-Net (see Figure 3(b)). Third, the MC-SG is the proposed pipeline (see Figure 3(c)). We first used M-SG to generate masks. We then used the generated masks by M-SG as conditions to make C-SG generate images. The generated samples from MC-SG were then employed with the real samples to train another U-Net for the downstream task.

3.4 Statistical Tests

We employed the Friedman test of equivalence on the evaluated metrics. It was used with the predictions made on the test set to compare the performances of the evaluated methods. Following Demšar [2006], we also detailed the significant differences between each pair of methods (*i.e.* better, worse, or undetermined) by a Nemenyi post-hoc test of pair-wise differences.

4 Experiments

4.1 Datasets

The experiment was conducted on six datasets, spanning a range of anatomies, medical imaging modalities, and dataset sizes, in order to evaluate the capabilities of the proposed method. Five of the datasets are accessible to the public as segmentation challenges. In addition to these public datasets, we made use of an in-house dataset collected at the University Hospital of Umeå, Umeå, Sweden.

Table 1: The datasets, augmentation, and experimental setup in this study. A depth of D means that the volume shape had a varied depth.

material/dataset	BraTS20	KiTS19	IBSR18	U-PRO	D-HEART	D-SPLEEN
type	MRI	CT	MRI	CT	MRI	CT
#modalities	4	1	1	1	1	1
#classes	3	2	3	3	1	1
#patients	369	210	18	500	20	41
#patients cases	{20, 50, 100, 200, 369}	{20, 50, 100, 210}	{18}	{20, 50, 100, 200, 500}	{20}	{20, 41}
original shape	240-240-155	512-512- D	256-128-256	512-512- D	320-320- D	512-512- D
resized shape	256-256-155	256-256- D	256-256-256	256-256- D	256-256- D	256-256- D
augmentation						
flip left-right	✓	✗	✓	✓	✗	✗
rotation	✓	✓	✓	✓	✓	✓
shift	✓	✓	✓	✓	✓	✓
zoom	✓	✓	✓	✓	✓	✓
training						
#epochs	70	70	150	70	150	150
optimizer	Adam	Adam	Adam	Adam	Adam	Adam
learning rate	$1 \cdot 10^{-4}$	$1 \cdot 10^{-4}$	$1 \cdot 10^{-4}$	$1 \cdot 10^{-4}$	$1 \cdot 10^{-4}$	$1 \cdot 10^{-4}$
batch-size	64	64	64	64	64	64

The Umeå Pelvic Region Organs (U-PRO) is an in-house dataset that contains CT scans of the pelvis region from 1 244 patients who had radiotherapy treatments for prostate cancer at the University Hospital of Umeå, Umeå, Sweden. The bladder and the rectum are two of the organs that are considered to be at risk. In addition to the bladder and rectum, the delineations also include the prostate, which is most of the time referred to as the clinical target volume. The separate structure

masks for these three aforementioned structures were combined into a single mask image, with the pixel value of 1 assigned to the prostate, 2 assigned to the bladder, and 3 assigned to the rectum. Patients who did not have all three structures were removed, leaving 1 148 patients. We then randomly selected 500 patients for this study.

In connection to the International Conference on Medical Image Computing and Computer Assisted Intervention (MICCAI) main event that took place in 2020, the *Brain Tumors in Multimodal Magnetic Resonance Imaging Challenge 2020 (BraTS20)* [Menze et al., 2014, Bakas et al., 2017] was organized as a satellite event. The BraTS20 dataset contains 369 volumes of three-dimensional (3D) multiple pre-operative MRI from 19 different hospitals that have either high grade glioma (HGG) or low grade glioma (LGG). The following MRI sequences were performed on each patient: T1-weighted (T1w), post-contrast T1-weighted (T1c), T2-weighted (T2w), and T2 Fluid Attenuated Inversion Recovery (FLAIR). These scans were performed utilizing various techniques and scanners, and the magnetic field strength was set to 3T. Several annotators were present to do manual segmentations. A contrast-enhancing tumor was differentiated from a necrotic and non-enhancing tumor core, as well as peritumoral edema. The skulls have been cropped out of the images. After that, the voxels were interpolated to a single size and co-registered to a single anatomical reference.

The *Internet Brain Segmentation Repository (IBSR18)* dataset [Cocosco et al., 1997] was released by the National Institute of Neurological Disorders and Stroke (NINDS). The dataset contains 18 three-dimensional T1-weighted MRI scans of 1.5mm slice thickness. Radiologists annotated the contours of the whole brain, including cerebrospinal fluid (label 1), gray matter (label 2), and white matter (label 3).

The *Kidney Tumor Segmentation Challenge 2019 (KiTS19)* was a grand challenge in conjunction with the MICCAI in 2019, which was held in Shenzhen, China [Heller et al., 2019]. The challenge aimed to autonomously segment contrast-enhanced CT images of the abdomen into three classes: kidney, tumor, and background. The patients included in this dataset were chosen randomly from those who had undergone radical nephrectomy at the University of Minnesota Medical Center between 2010 and 2018.

The *Spleen Segmentation Decathlon (D-SPLEEN)* dataset is one out of ten labeled datasets provided by the Medical Segmentation Decathlon that covers a wide range of organs [Simpson et al., 2019]. The D-SPLEEN dataset’s region of interest (ROI) target is the spleen. The dataset initially belonged to a study on splenic volume change following chemotherapy in patients with liver metastases and consists of 41 CT scans with annotated masks.

The *Heart Segmentation Decathlon (D-HEART)* is a small dataset and is also part of Medical Segmentation Decathlon [Simpson et al., 2019]. The D-HEART dataset contains 20 mono-modal MRI scans with annotated masks. The ROI target of this dataset is the left atrium.

4.2 Experiments

We carried out the experiments on six datasets (see Section 4.1). To evaluate the capability of evaluated methods on diverse datasets sizes, we randomly selected several number of samples from each dataset to form new sub-datasets with specific sizes. Row “#patients cases” in Table 1 shows the numbers of patients that were randomly selected. For example, the 20, 41 of the D-SPLEEN means that we created two distinguish sub-datasets from the D-SPLEEN dataset: one dataset had 20 samples, and the other had 41 samples.

In order to evaluate the effect of the fraction of generated training samples for the segmentation task, we trained multiple U-Nets for the different number of generated samples (by the B-SG and the MC-SG, see Section 3.3). The numbers of generated samples were 20, 50, 100, 200, 400, and 500 patients. Consequently, each pipeline that used generated samples from GAN had 6 variants, and each variant corresponded to a number of generated patients.

We also applied simple data augmentation techniques (spatial transformations) to each U-Net model. Hence, we ended up with 26 methods in total, *i.e.* (BL+6 variants of B-SG+6 variants of MC-SG) × (2 data augmentation), see Table 2.

4.3 Evaluation

To measure the difference between two Gaussian distributions, Fréchet [1957] presented the Fréchet distance. Inspired by that work, Heusel et al. [2017] proposed Fréchet Inception Distance (FID) to evaluate the quality of generated samples of GANs. In this work, we used FID to evaluate the GANs. The FID is computed as

$$d^2((\boldsymbol{\mu}, \boldsymbol{\Sigma}), (\boldsymbol{\mu}_g, \boldsymbol{\Sigma}_g)) = \|\boldsymbol{\mu} - \boldsymbol{\mu}_g\|_2^2 + \text{tr}(\boldsymbol{\Sigma} + \boldsymbol{\Sigma}_g - 2(\boldsymbol{\Sigma}\boldsymbol{\Sigma}_g)^{1/2}), \quad (4)$$

where tr denotes trace of a matrix. The $\|\cdot\|_2$ is the standard ℓ_2 norm. The $d(\cdot, \cdot)$ denotes the Fréchet distance between two Gaussian distributions. The $(\boldsymbol{\mu}, \boldsymbol{\Sigma})$ and $(\boldsymbol{\mu}_g, \boldsymbol{\Sigma}_g)$ are the mean and covariance matrices of Gaussian distributions fitted to the feature representations of real and generated images, respectively. The feature representations (2048-length vectors) is computed by feeding the images to an Inception-v3 network [Szegedy et al., 2015] that was pre-trained on the ImageNet dataset [Krizhevsky et al., 2012].

We used the soft Sørensen-Dice coefficient (DSC) loss in the downstream tasks (*i.e.* segmentation). The soft DSC loss has been used in many previous works, *e.g.* by Milletari et al. [2016], Vu et al. [2020a,b, 2021b,a]. The soft DSC loss is computed as

$$\mathcal{L}_{\text{DSC}}(\mathbf{M}, \hat{\mathbf{M}}) = \frac{-2 \sum_{i=1}^N m_i \hat{m}_i + \epsilon}{\sum_{i=1}^N m_i + \sum_{i=1}^N \hat{m}_i + \epsilon}, \quad (5)$$

where \hat{m}_i is the i -th element of the predicted softmax output of the network, and the m_i is the i -th element of a one-hot encoding of the ground truth labels. To avoid division by zero, we added $\epsilon = 1 \cdot 10^{-5}$ to the denominator. We also added ϵ to the numerator to give true zero predicted masks a score of 1

We evaluated the segmentation tasks using the DSC, which is calculated as

$$\text{DSC}(\mathbf{M}, \hat{\mathbf{M}}) = -\mathcal{L}_{\text{DSC}}(\mathbf{M}, \hat{\mathbf{M}}). \quad (6)$$

in which ϵ is set to zero.

4.4 Implementation Details and Training

The proposed method was implemented in PyTorch 1.10¹. The experiments were run on NVIDIA Tesla K80 and V100 GPUs housed at the High Performance Computer Center North (HPC2N)² at Umeå University, Sweden.

We used the Adam optimizer [Kingma and Ba, 2015] in all experiments, with a fixed learning rate of $1 \cdot 10^{-4}$ (see Table 1). The number of epochs for each experiment was set at 70 or 150, *i.e.* depending on the datasets. We used the two-dimensional (2D) U-Net [Ronneberger et al., 2015] for the segmentation tasks. Batch normalization was used after all convolutional layers: in the transition blocks and in the main network. The transition blocks (downsampling or upsampling) consist of a batch normalization layer, a rectified linear unit (RELU) layer, and a convolution layer.

Except for the D-SPLEEN, all datasets were standardized to zero-mean and unit variance. Before normalization, N4ITK bias field correction [Tustison et al., 2010] was applied to the BraTS20 dataset. Samples from the D-SPLEEN dataset were rescaled to $[-1, 1]$.

To artificially enlarge the D-SPLEEN and BraTS20 dataset size and increase the variability in the data, we applied different on-the-fly data augmentations. Those were: horizontal flipping, rotation within a range of -1 to 1 degrees, rescaling with a factor of 0.9 to 1.1 , and shifting the images by -5 to 5 percent.

5 Results and Discussion

Figure 4 shows an uncurated set of generated samples from the BraTS20 dataset using the generator of B-SG. From left to right, the figure illustrates the T1w, T2w, FLAIR, T1c and corresponding

¹<https://pytorch.org/>

²<https://www.hpc2n.umu.se/>

label mask. From Figure 4, we can see that the average quality of the generated sample is not high. In specific, though the generated images have good structures, including lateral ventricles, third ventricle, thalamus, basal ganglia, brain lobes, tumor regions, and so on; however, when zooming in, we can see that the images look quite blotchy and blurry with low-quality.

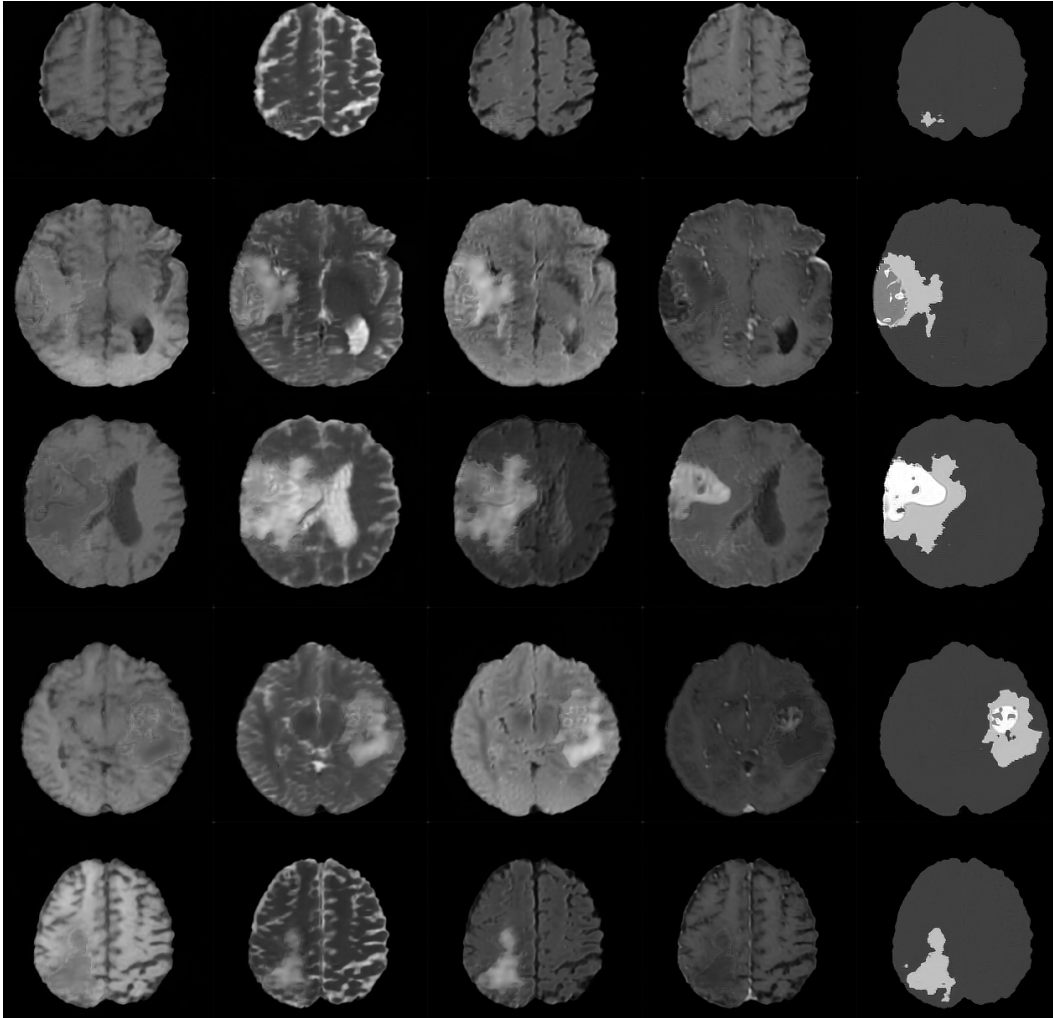


Figure 4: An uncurated set of generated samples from the BraTS20 dataset using the generator of B-SG. From left to right: T1w, T2w, FLAIR, T1c and the corresponding label mask.

Figure 5 presents the DSC scores and their standard errors of 26 models on 18 datasets (see Table 2) with different numbers of added generated patients. The titles of subfigures present the datasets’ names. For example, BraTS20-20 shows that this dataset was created by randomly selecting 20 patients from the BraTS20 dataset. The x -axis of all subfigures indicates the number of added generated patients/volumes. When the “# gen. samples” is equivalent to zero, it represents the baseline (*i.e.*, training without generated samples, see figure 3(a)). The “w. aug.” and “w.o. aug.” stand for with and without data augmentation—the process of artificially enlarging the size of the training dataset by producing modified versions of the available images.

Table 2 shows the Nemenyi post-hoc test comparing all evaluated methods (row) on all datasets (column). The number in the table presents the sum of Nemenyi directions where (+) and (−) mean adding and subtracting one unit, respectively. The Nemenyi directions include (−), (+) and (0). The minus (−) means ranked significantly lower. The zero (0) means no significant difference. The plus (+) means ranked significantly higher when comparing a method to another method (see *e.g.*, Table 3). From Table 2, we can determine how well a method compares to other evaluated methods.

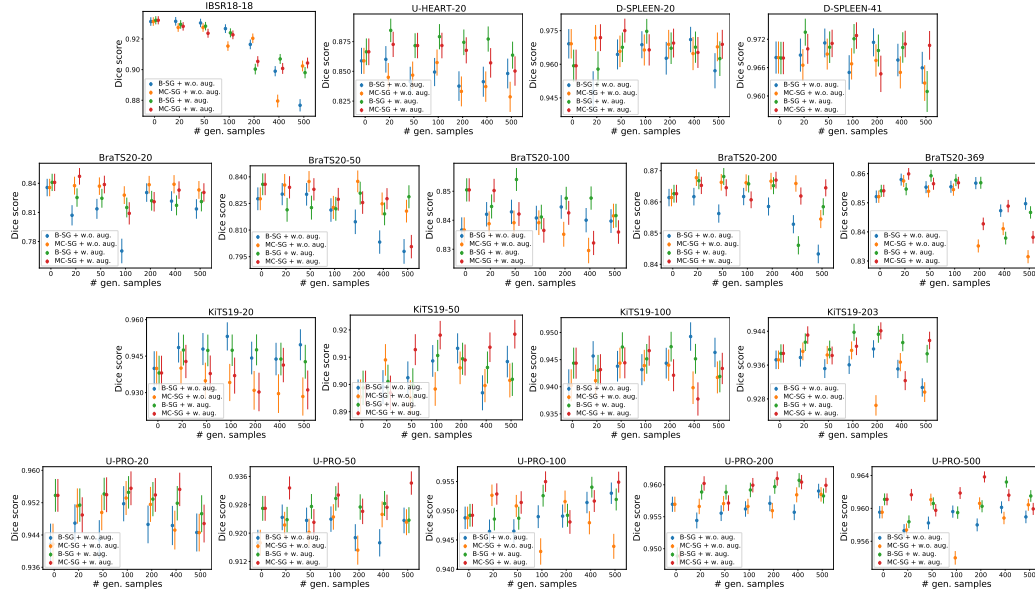


Figure 5: Comparison of DSC scores and their standard errors of 26 models on 18 datasets (see Table 2) with different numbers of added generated patients. The titles of subfigures present the datasets’ names. The x -axis of all subfigures shows the number of added generated patients/volumes.

Table 2: The results of the Nemenyi post-hoc test comparing all evaluated methods on all datasets. The directions include (–), (+) and (0). A minus (–) means ranked significantly lower. A zero (0) means no significant difference. A plus (+) means ranked significantly higher when comparing a method to another. The number in the table presents the sum of Nemenyi directions where (+) and (–) mean adding and subtracting one unit, respectively.

Models	U-HEART-20	D-SPLEEN-20	D-SPLEEN-41	IBSR 18-18	KiTS 19-20	KiTS 19-50	KiTS 19-100	KiTS 19-203	BraTS20-20	BraTS20-50	BraTS20-100	BraTS20-200	BraTS20-369	U-PRO-20	U-PRO-50	U-PRO-100	U-PRO-200	U-PRO-500
BL + w.o.	0	0	0	10	0	0	0	0	0	0	0	0	1	0	0	0	0	0
B-SG + w.o. + 20	0	0	0	10	0	0	0	0	0	0	0	0	4	0	0	0	0	0
B-SG + w.o. + 50	0	0	0	10	0	0	0	0	0	0	0	0	3	0	0	0	0	0
B-SG + w.o. + 100	0	0	0	6	0	0	0	0	0	0	0	0	3	0	0	0	0	0
B-SG + w.o. + 200	0	0	0	2	0	0	0	0	0	0	0	0	4	0	0	0	0	0
B-SG + w.o. + 400	0	0	0	-14	0	0	0	0	0	0	0	0	0	0	0	0	0	0
B-SG + w.o. + 500	0	0	0	-20	0	0	0	0	0	0	0	0	0	0	0	0	0	0
MC-SG + w.o. + 20	0	0	0	9	0	0	0	0	0	0	0	0	4	0	0	0	0	0
MC-SG + w.o. + 50	0	0	0	6	0	0	0	0	0	0	0	0	1	0	0	0	0	0
MC-SG + w.o. + 100	0	0	0	2	0	0	0	0	0	0	0	0	1	0	0	0	0	0
MC-SG + w.o. + 200	0	0	0	3	0	0	0	0	0	0	0	0	-12	0	0	0	0	0
MC-SG + w.o. + 400	0	0	0	-16	0	0	0	0	0	0	0	0	0	0	0	0	0	0
MC-SG + w.o. + 500	0	0	0	-6	0	0	0	0	0	0	0	0	-16	0	0	0	0	0
BL + w.	0	0	0	10	0	0	0	0	0	0	0	0	1	0	0	0	0	0
B-SG + w. + 20	0	0	0	10	0	0	0	0	0	0	0	0	3	0	0	0	0	0
B-SG + w. + 50	0	0	0	8	0	0	0	0	0	0	0	0	4	0	0	0	0	0
B-SG + w. + 100	0	0	0	5	0	0	0	0	0	0	0	0	4	0	0	0	0	0
B-SG + w. + 200	0	0	0	-12	0	0	0	0	0	0	0	0	4	0	0	0	0	0
B-SG + w. + 400	0	0	0	-6	0	0	0	0	0	0	0	0	-7	0	0	0	0	0
B-SG + w. + 500	0	0	0	-12	0	0	0	0	0	0	0	0	0	0	0	0	0	0
MC-SG + w. + 20	0	0	0	6	0	0	0	0	0	0	0	0	4	0	0	0	0	0
MC-SG + w. + 50	0	0	0	5	0	0	0	0	0	0	0	0	3	0	0	0	0	0
MC-SG + w. + 100	0	0	0	3	0	0	0	0	0	0	0	0	3	0	0	0	0	0
MC-SG + w. + 200	0	0	0	-5	0	0	0	0	0	0	0	0	0	0	0	0	0	0
MC-SG + w. + 400	0	0	0	-10	0	0	0	0	0	0	0	0	0	0	0	0	0	0
MC-SG + w. + 500	0	0	0	-4	0	0	0	0	0	0	0	0	-12	0	0	0	0	0

From Table 2, we can see that there are only two datasets that we can determine the significant differences from the methods, which are IBSR18-18 and BraTS20-369. For the other datasets, the differences between evaluated methods are non-significant (all zeros), *i.e.*, the segmentation networks

did not benefit from the generated images by the proposed GANs. Looking at the IBSR18-18 and BraTS20-369 in Table 2, it is apparent that the baselines with and without data augmentation are among the top-performing methods. Another observation is that adding many generated images did not improve the performance; otherwise, it was even worse in some cases, *e.g.*, “B-SG w.o. + 500”.

Table 3: The results of the Nemenyi post-hoc test comparing all evaluated methods on the BraTS20-369. A minus (−) means ranked significantly lower, a zero (0) means non-significant difference, and a plus (+) means ranked significantly higher, when comparing a method in the rows to a method in the columns. “BL” is the baseline (training without generated images). “B-SG” is the StyleGAN2. “MC-SG” is the proposed method. The “w.o.” denotes without augmentation, while the “w.” denotes with augmentation. The number following after “+ w.” or “+ w.” is the number of generated patients.

	BL + w.o.	B-SG + w.o. + 20	B-SG + w.o. + 50	B-SG + w.o. + 100	B-SG + w.o. + 200	B-SG + w.o. + 400	B-SG + w.o. + 500	MC-SG + w.o. + 20	MC-SG + w.o. + 50	MC-SG + w.o. + 100	MC-SG + w.o. + 200	MC-SG + w.o. + 400	MC-SG + w.o. + 500	BL + w.	B-SG + w. + 20	B-SG + w. + 50	B-SG + w. + 100	B-SG + w. + 200	B-SG + w. + 400	B-SG + w. + 500	MC-SG + w. + 20	MC-SG + w. + 50	MC-SG + w. + 100	MC-SG + w. + 200	MC-SG + w. + 400	MC-SG + w. + 500	Score	
BL + w.o.	0	0	0	0	0	0	0	0	0	0	0	0	0	+	0	0	0	0	0	0	0	0	0	0	0	0	1	
B-SG + w.o. + 20	0	0	0	0	0	0	0	0	0	0	0	+	0	0	0	0	0	0	0	0	+	0	0	0	0	0	+	4
B-SG + w.o. + 50	0	0	0	0	0	0	0	0	0	0	0	+	0	0	0	0	0	0	0	0	0	0	0	0	0	0	+	3
B-SG + w.o. + 100	0	0	0	0	0	0	0	0	0	0	0	+	0	0	0	0	0	0	0	0	0	0	0	0	0	0	+	3
B-SG + w.o. + 200	0	0	0	0	0	0	0	0	0	0	0	+	0	0	0	0	0	0	0	0	+	0	0	0	0	0	+	4
B-SG + w.o. + 400	0	0	0	0	0	0	0	0	0	0	0	+	0	0	0	0	0	0	0	0	0	0	0	0	0	0	0	0
B-SG + w.o. + 500	0	0	0	0	0	0	0	0	0	0	0	+	0	0	0	0	0	0	0	0	0	0	0	0	0	0	0	0
MC-SG + w.o. + 20	0	0	0	0	0	0	0	0	0	0	0	+	0	0	0	0	0	0	0	0	+	0	0	0	0	0	+	4
MC-SG + w.o. + 50	0	0	0	0	0	0	0	0	0	0	0	+	0	0	0	0	0	0	0	0	0	0	0	0	0	0	0	1
MC-SG + w.o. + 100	0	0	0	0	0	0	0	0	0	0	0	+	0	0	0	0	0	0	0	0	0	0	0	0	0	0	0	1
MC-SG + w.o. + 200	0	−	−	−	−	−	−	−	−	−	−	−	−	−	−	−	−	−	−	−	−	−	−	−	−	−	−	-12
MC-SG + w.o. + 400	0	0	0	0	0	0	0	0	0	0	0	0	0	0	0	0	0	0	0	0	0	0	0	0	0	0	0	0
MC-SG + w.o. + 500	−	−	−	−	−	−	−	−	−	−	−	−	−	−	−	−	−	−	−	−	−	−	−	−	−	−	−	-16
BL + w.	0	0	0	0	0	0	0	0	0	0	0	+	0	0	0	0	0	0	0	0	0	0	0	0	0	0	1	
B-SG + w. + 20	0	0	0	0	0	0	0	0	0	0	0	+	0	0	0	0	0	0	0	0	0	0	0	0	0	0	+	3
B-SG + w. + 50	0	0	0	0	0	0	0	0	0	0	0	+	0	0	0	0	0	0	0	0	0	0	0	0	0	0	+	4
B-SG + w. + 100	0	0	0	0	0	0	0	0	0	0	0	+	0	0	0	0	0	0	0	0	0	0	0	0	0	0	+	4
B-SG + w. + 200	0	0	0	0	0	0	0	0	0	0	0	+	0	0	0	0	0	0	0	0	+	0	0	0	0	0	+	4
B-SG + w. + 400	0	−	0	0	−	0	0	−	0	0	0	0	0	−	−	−	−	−	−	−	−	−	−	−	−	−	−	-7
B-SG + w. + 500	0	0	0	0	0	0	0	0	0	0	0	0	0	0	0	0	0	0	0	0	0	0	0	0	0	0	0	0
MC-SG + w. + 20	0	0	0	0	0	0	0	0	0	0	0	+	0	0	0	0	0	0	0	0	+	0	0	0	0	0	+	4
MC-SG + w. + 50	0	0	0	0	0	0	0	0	0	0	0	+	0	0	0	0	0	0	0	0	0	0	0	0	0	0	+	3
MC-SG + w. + 100	0	0	0	0	0	0	0	0	0	0	0	+	0	0	0	0	0	0	0	0	0	0	0	0	0	0	+	3
MC-SG + w. + 200	0	0	0	0	0	0	0	0	0	0	0	0	0	0	0	0	0	0	0	0	0	0	0	0	0	0	0	0
MC-SG + w. + 400	0	0	0	0	0	0	0	0	0	0	0	0	0	0	0	0	0	0	0	0	0	0	0	0	0	0	0	0
MC-SG + w. + 500	0	−	−	−	−	−	−	−	−	−	−	−	−	−	−	−	−	−	−	−	−	−	−	−	−	−	−	-12

6 Conclusion

In this work, we introduced a novel conditional Generative Adversarial Network based on the standard StyleGAN2 to generate high-quality medical images with different modalities. We evaluated the quality of the generated medical images and the effect of this augmentation on the segmentation performance. There are, in fact, more investigations and experiments needed for conclusions on the effect of generated images on the downstream segmentation task.

References

- Karim Armanious, Youssef Mecky, Sergios Gatidis, and Bin Yang. Adversarial inpainting of medical image modalities. In *ICASSP 2019-2019 IEEE International Conference on Acoustics, Speech and Signal Processing (ICASSP)*, pages 3267–3271. IEEE, 2019.
- Oleksandr Bailo, DongShik Ham, and Young Min Shin. Red blood cell image generation for data augmentation using Conditional Generative Adversarial Networks. In *Proceedings of the IEEE/CVF Conference on Computer Vision and Pattern Recognition (CVPR) workshops*, pages 0–0, 2019.
- Spyridon Bakas, Hamed Akbari, Aristeidis Sotiras, Michel Bilello, Martin Rozycki, Justin S Kirby, John B Freymann, Keyvan Farahani, and Christos Davatzikos. Advancing The Cancer Genome Atlas glioma MRI collections with expert segmentation labels and radiomic features. *Scientific data*, 4:170117, 2017.

- Christopher Bowles, Liang Chen, Ricardo Guerrero, Paul Bentley, Roger Gunn, Alexander Hammers, David Alexander Dickie, Maria Valdés Hernández, Joanna Wardlaw, and Daniel Rueckert. GAN Augmentation: Augmenting Training Data using Generative Adversarial Networks. *arXiv preprint arXiv:1810.10863*, 2018.
- Francesco Calimeri, Aldo Marzullo, Claudio Stamile, and Giorgio Terracina. Biomedical Data Augmentation Using Generative Adversarial Neural Networks. In *International Conference on Artificial Neural Networks*, pages 626–634. Springer, 2017.
- Chris A Cocosco, Vasken Kollokian, Remi K-S Kwan, G Bruce Pike, and Alan C Evans. Brainweb: Online interface to a 3D MRI simulated brain database. In *NeuroImage*, volume 5, page 425, 1997.
- Janez Demšar. Statistical comparisons of classifiers over multiple data sets. *Journal of Machine Learning Research*, 7:1–30, 2006. ISSN 15337928.
- Jia Deng, Wei Dong, Richard Socher, Li-Jia Li, Kai Li, and Li Fei-Fei. ImageNet: A large-scale hierarchical image database. In *2009 IEEE Conference on Computer Vision and Pattern Recognition*, pages 248–255. Ieee, 2009.
- Maurice Fréchet. Sur la distance de deux lois de probabilité. *Comptes Rendus Hebdomadaires des Seances de L Academie des Sciences*, 244(6):689–692, 1957.
- Leon Gatys, Alexander Ecker, and Matthias Bethge. A Neural Algorithm of Artistic Style. *Journal of Vision*, 16(12):326–326, 2016.
- Ian Goodfellow, Jean Pouget-Abadie, Mehdi Mirza, Bing Xu, David Warde-Farley, Sherjil Ozair, Aaron Courville, and Yoshua Bengio. Generative Adversarial Nets. In Z. Ghahramani, M. Welling, C. Cortes, N. Lawrence, and K.Q. Weinberger, editors, *Advances in Neural Information Processing Systems*, volume 2, page 2672–2680. Curran Associates, Inc., 2014.
- Zhongyi Han, Benzhen Wei, Ashley Mercado, Stephanie Leung, and Shuo Li. Spine-GAN: Semantic segmentation of multiple spinal structures. *Medical image analysis*, 50:23–35, 2018.
- Kaiming He, Xiangyu Zhang, Shaoqing Ren, and Jian Sun. Deep Residual Learning for Image Recognition. *2016 IEEE Conference on Computer Vision and Pattern Recognition (CVPR)*, pages 770–778, 2016.
- Nicholas Heller, Niranjana Sathianathan, Arveen Kalapara, Edward Walczak, Keenan Moore, Heather Kaluzniak, Joel Rosenberg, Paul Blake, Zachary Rengel, Makinna Oestreich, et al. The KiTS19 Challenge Data: 300 Kidney Tumor Cases with Clinical Context, CT Semantic Segmentations, and Surgical Outcomes. *arXiv preprint arXiv:1904.00445*, 2019.
- Martin Heusel, Hubert Ramsauer, Thomas Unterthiner, Bernhard Nessler, and Sepp Hochreiter. GANs Trained by a Two Time-Scale Update Rule Converge to a Local Nash Equilibrium. *Advances in neural information processing systems*, 30, 2017.
- Phillip Isola, Jun-Yan Zhu, Tinghui Zhou, and Alexei A Efros. Image-to-Image Translation with Conditional Adversarial Nets. In *Proceedings of the IEEE Conference on Computer Vision and Pattern Recognition*, pages 1125–1134, 2017.
- Tero Karras, Timo Aila, Samuli Laine, and Jaakko Lehtinen. Progressive Growing of GANs for Improved Quality, Stability, and Variation. In *6th International Conference on Learning Representations (ICLR)*, pages 1–26, 2018a.
- Tero Karras, Samuli Laine, and Timo Aila. A Style-Based Generator Architecture for Generative Adversarial Networks. *IEEE Transactions on Pattern Analysis and Machine Intelligence*, 43(12): 4217–4228, 2018b. ISSN 19393539.
- Tero Karras, Miika Aittala, Janne Hellsten, Samuli Laine, Jaakko Lehtinen, and Timo Aila. Training Generative Adversarial Networks with Limited Data. In *Proceedings of the 34th International Conference on Neural Information Processing Systems (NeurIPS)*, NIPS’20, page 12104–12114, Red Hook, NY, USA, 2020a. Curran Associates Inc. ISBN 9781713829546.

- Tero Karras, Samuli Laine, Miika Aittala, Janne Hellsten, Jaakko Lehtinen, and Timo Aila. Analyzing and improving the image quality of stylegan. In *IEEE Conference on Computer Vision and Pattern Recognition (CVPR)*, pages 8107–8116, 2020b.
- Tero Karras, Miika Aittala, Samuli Laine, Erik Härkönen, Janne Hellsten, Jaakko Lehtinen, and Timo Aila. Alias-Free Generative Adversarial Networks. In M. Ranzato, A. Beygelzimer, Y. Dauphin, P.S. Liang, and J. Wortman Vaughan, editors, *Proceedings of the 35th Advances in Neural Information Processing Systems (NeurIPS)*, volume 34 of *NIPS'21*, pages 852–863, Red Hook, NY, USA, 2021. Curran Associates, Inc.
- Sunho Kim, Byungjai Kim, and Hyun Wook Park. Synthesis of brain tumor multicontrast MR images for improved data augmentation. *Medical Physics*, 48(5):2185–2198, 2021. ISSN 00942405.
- Diederik P Kingma and Jimmy Ba. Adam: A Method for Stochastic Optimization. In *7th International Conference on Learning Representations (ICLR)*, 2015.
- Alex Krizhevsky, Ilya Sutskever, and Geoffrey E Hinton. ImageNet Classification with Deep Convolutional Neural Networks. In *Advances in Neural Information Processing Systems (NeurIPS)*, pages 1097–1105, 2012.
- Niklas Kühl, Marc Goutier, Lucas Baier, Clemens Wolff, and Dominik Martin. Human vs. supervised machine learning: Who learns patterns faster? *Cognitive Systems Research*, 76:78–92, 2022.
- Ali Madani, Mehdi Moradi, Alexandros Karargyris, and Tanveer Syeda-Mahmood. Chest x-ray generation and data augmentation for cardiovascular abnormality classification. In *Medical imaging 2018: Image processing*, volume 10574, pages 415–420. SPIE, 2018.
- Bjoern H Menze, Andras Jakab, Stefan Bauer, Jayashree Kalpathy-Cramer, Keyvan Farahani, Justin Kirby, Yuliya Burren, Nicole Porz, Johannes Slotboom, Roland Wiest, et al. The Multimodal Brain Tumor Image Segmentation Benchmark (BRATS). *IEEE Transactions on Medical Imaging*, 34(10):1993–2024, 2014.
- F. Milletari, N. Navab, and S. Ahmadi. V-Net: Fully Convolutional Neural Networks for Volumetric Medical Image Segmentation. In *Fourth International Conference on 3D Vision (3DV)*, pages 565–571, 2016.
- Mehdi Mirza and Simon Osindero. Conditional Generative Adversarial Nets. *arXiv preprint arXiv:1411.1784*, 2014.
- Saman Motamed, Patrik Rogalla, and Farzad Khalvati. Data augmentation using Generative Adversarial Networks (GANs) for GAN-based detection of Pneumonia and COVID-19 in chest X-ray images. *Informatics in Medicine Unlocked*, 27:100779, 2021.
- Augustus Odena, Christopher Olah, and Jonathon Shlens. Conditional image synthesis with auxiliary classifier GANs. In *Proceedings of the 34th International Conference on Machine Learning-Volume 70*, pages 2642–2651, 2017.
- Olaf Ronneberger, Philipp Fischer, and Thomas Brox. U-Net: Convolutional Networks for Biomedical Image Segmentation. In *International Conference on Medical Image Computing and Computer Assisted Intervention*, pages 234–241. Springer, 2015.
- Veit Sandfort, Ke Yan, Perry J. Pickhardt, and Ronald M. Summers. Data augmentation using generative adversarial networks (CycleGAN) to improve generalizability in CT segmentation tasks. *Scientific Reports*, 9(1):1–9, 2019. ISSN 20452322.
- Connor Shorten and Taghi M Khoshgoftaar. A survey on image data augmentation for deep learning. *Journal of Big Data*, 6(1):1–48, 2019.
- Amber L Simpson, Michela Antonelli, Spyridon Bakas, Michel Bilello, Keyvan Farahani, Bram Van Ginneken, Annette Kopp-Schneider, Bennett A Landman, Geert Litjens, Bjoern Menze, et al. A large annotated medical image dataset for the development and evaluation of segmentation algorithms. *arXiv preprint arXiv:1902.09063*, 2019.

- Youssef Skandarani, Pierre-Marc Jodoin, and Alain Lalande. Gans for medical image synthesis: An empirical study. *arXiv preprint arXiv:2105.05318*, 2021.
- Christian Szegedy, Wei Liu, Yangqing Jia, Pierre Sermanet, Scott Reed, Dragomir Anguelov, Dumitru Erhan, Vincent Vanhoucke, and Andrew Rabinovich. Going deeper with convolutions. In *2015 IEEE Conference on Computer Vision and Pattern Recognition (CVPR)*, pages 1–9, 2015.
- Nicholas J Tustison, Brian B Avants, Philip A Cook, Yuanjie Zheng, Alexander Egan, Paul A Yushkevich, and James C Gee. N4ITK: Improved N3 Bias Correction. *IEEE Transactions on Medical Imaging*, 29(6):1310, 2010.
- Minh H Vu, Guus Grimbergen, Tufve Nyholm, and Tommy Löfstedt. Evaluation of multislice inputs to convolutional neural networks for medical image segmentation. *Medical Physics*, 47(12): 6216–6231, 2020a.
- Minh H Vu, Tufve Nyholm, and Tommy Löfstedt. TuNet: End-to-end Hierarchical Brain Tumor Segmentation using Cascaded Networks. In *Brainlesion: Glioma, Multiple Sclerosis, Stroke and Traumatic Brain Injuries*, volume 11992, pages 174–186. Springer International Publishing, 2020b.
- Minh H Vu, Gabriella Norman, Tufve Nyholm, and Tommy Löfstedt. A Data-Adaptive Loss Function for Incomplete Data and Incremental Learning in Semantic Image Segmentation. *IEEE Transactions on Medical Imaging*, 41(6):1320–1330, 2021a.
- Minh H Vu, Tufve Nyholm, and Tommy Löfstedt. Multi-Decoder Networks with Multi-Denoising Inputs for Tumor Segmentation. In *Brainlesion: Glioma, Multiple Sclerosis, Stroke and Traumatic Brain Injuries*, volume 12658, pages 412–423. Springer International Publishing, 2021b.
- Jun-Yan Zhu, Taesung Park, Phillip Isola, and Alexei A. Efros. Unpaired Image-to-Image Translation Using Cycle-Consistent Adversarial Networks. In *2017 IEEE International Conference on Computer Vision (ICCV)*, pages 2242–2251, 2017.